Transient dispersion in a channel with crossflow and wall adsorption

Bohan Wang [1], Weiquan Jiang [2,3], Guoqian Chen [1,3,*] and Luoyi Tao [4,†]
[1]*Laboratory of Systems Ecology and Sustainability Science, College of Engineering, Peking University, Beijing 100871, China*
[2]*State Key Laboratory of Hydroscience and Engineering, Department of Hydraulic Engineering, Tsinghua University, Beijing 100084, China*
[3]*Macao Environmental Research Institute, Macau University of Science and Technology, Macao 999078, China*
[4]*Department of Aerospace Engineering, Indian Institute of Technology Madras, Chennai 60036, India*

(Received 30 April 2022; accepted 7 July 2022; published 18 July 2022)

Dispersion of substances with reactive boundaries is relevant to a wide range of chemical, biological, and geophysical processes. A supplied crossflow, or equivalently sedimentation of the substance, is also expected to affect the dispersion process. We consider a setting with two infinite parallel plates, where the diffusive substance is adsorbed at the lower plate, simultaneously advected longitudinally by a main flow and vertically by a crossflow. Although the same configuration has been studied previously with the generalized Taylor dispersion (GTD) theory [M. Shapiro and H. Brenner, AIChE J. **33**, 1155 (1987)] and a dual-perturbation method [T. Y. Lin and E. S. G. Shaqfeh, Phys. Rev. Fluids **4**, 034501 (2019)], both of them focused on the long-time asymptotic dispersion regime, exclusive of the important transient dispersion process. As an extension of these works to the transient dispersion process, we utilize the classical method of moments along with the eigenfunction expansion to calculate the moments up to fourth order, and thus the effects of non-Gaussian properties can be reflected. Compared with the result of Brownian dynamics simulations, the present work is shown sufficient to cover the preasymptotic dispersion regime out of reach of the GTD and dual-perturbation method. Strong non-Gaussian properties are found in the preasymptotic regime, as reflected by the nonzero skewness and kurtosis as well as asymmetric longitudinal concentration distribution. Additionally, it is found that the duration of the preasymptotic regime is extended in the presence of both the crossflow and wall adsorption. Considering that most of the substance may have been adsorbed during the preasymptotic regime, it is necessary to use higher-order dispersion models such as the one presented herein.

DOI: 10.1103/PhysRevFluids.7.074501

I. INTRODUCTION

Dispersion of a substance refers to the enhanced streamwise spreading due to the combined effect of molecular/turbulent diffusion and flow shear in the cross section. Specifically, when a substance diffuses in the transverse direction across streamlines, it samples different longitudinal velocities and, hence, spreads in the longitudinal direction much more than it would by molecular diffusion

*gqchen@pku.edu.cn
†luoyitao@iitm.ac.in

alone. This phenomenon was first studied by Taylor [1], and is therefore also known as "Taylor dispersion." Taylor dispersion plays an important role in many natural processes and industrial applications such as mixing in natural flows [2–4], chemical engineering [5,6], and biological transport [7–11].

In Taylor's seminal works [1,12] regarding dispersion in either laminar or turbulent pipe flows, the dispersion mechanism originates from the diffusion (molecular or turbulent) and shear in the confining cross section. Taylor dispersion is subsequently extended to cover diverse applications and effects, including those with porous media, active particles, and reactive boundaries. A comprehensive framework was established by Frankel and Brenner [13], who named their generalization as "generalized Taylor dispersion" (GTD) theory, as elaborated in a later textbook [14].

While Taylor's analysis of the dispersion process seems to be largely based on his ingenious intuition, Aris [15] introduced the method of moments and gave a more analytical derivation of the asymptotic dispersion coefficients ["asymptotic" implies that the longitudinal distribution of cross-sectional mean concentration has reached Gaussian, and the dispersion coefficients (drift and dispersivity) have reached a steady state]. It is noted that the GTD is also based on Aris' asymptotic moment analysis, but GTD is able to encompass more complex configurations such as porous media, nonspherical particles, sedimentation, and bulk/boundary reaction, by identifying the local space and global space [13]. The method of moments was extended to calculate the preasymptotic moments by Barton [16], who used the separation of variables and gave general expressions of the first four moments. There are also other methods of Taylor dispersion analysis, such as Gill's generalized model [17–21], homogenization technique [22–24], perturbation expansion [25], and asymptotic expansion [26].

Wall adsorption, or more generally an interfacial mass-transfer process, widely exists in flows with porous walls [27,28] and is relevant to many applications, such as separation of substance by chromatography [18], adsorption of solute in wetland substrate [29], and exchange between sediment and bedload [30,31]. In some applications, a crossflow can be supplied to enhance the filtration efficiency [32], or a sedimentation speed should be considered when investigating a heavy substance such as sediment. Physically and mathematically, both the crossflow and sedimentation are reflected by adding a vertical drift speed to the substance.

Jayaraj and Subramanian [33] analyzed the dispersion with a vertical drift speed numerically and compared with second-order Gill's generalized model (which only gives the asymptotic dispersion coefficients and resembles Taylor's classical model), they found the strong asymmetry of the longitudinal distribution of vertical average concentration at intermediate times (Fig. 3 in their work), suggesting the need to retain higher-order terms reflecting asymmetry in the dispersion model. Focusing on the dispersion with a vertical drift speed and wall adsorption, Smith [34] used a Gaussian approximation for the two-dimensional concentration distribution, i.e., assuming the longitudinal distribution of concentration at each vertical position is Gaussian but different vertical positions have different mean and variance. It is expected that the work of Smith [34] can incorporate non-Gaussian properties of the longitudinal distribution of vertical average concentration to some extent, although not consistent with the non-Gaussian longitudinal concentration distribution at each vertical position before the long-time limit.

In this work, we follow the problem setting in Lin and Shaqfeh [35], i.e., a canonical pressure-driven flow between two parallel plates supplied by a uniform and downwelling crossflow; in the meantime, the dispersing substance experiences different boundary conditions on the two plates: there is no reaction at the top boundary, whereas there is a first-order adsorption reaction at the bottom boundary. Although Lin and Shaqfeh [35] gave an analytical analysis of the dispersion process, they focused on the long-time asymptotic dispersion regime, which means the longitudinal concentration distribution has already been Gaussian. In addition, because Lin and Shaqfeh [35] used a dual-perturbation method, which requires a relatively weak adsorption rate as a small quantity, their results were not meant to be applicable for a situation with a moderate to high adsorption rate. It is also noteworthy that Shapiro and Brenner [36] have also considered an almost equivalent configuration, where the crossflow was replaced by a sedimentation speed of the particles

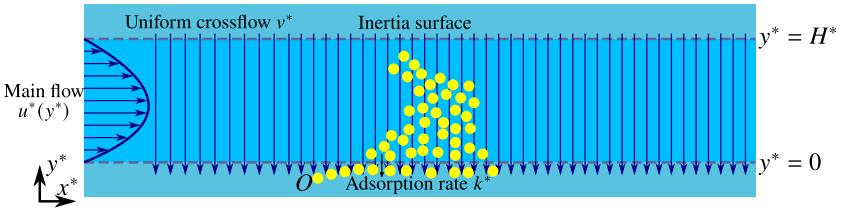

FIG. 1. The sketch of the problem setting.

and the longitudinal velocity profile was replaced by a Poiseuille flow. Nevertheless, they employed the GTD method and was therefore also intended for the long-time asymptotic dispersion regime.

Using the classical method of moments [15] supported by Barton's technical route (separation of variables) [16], we analyze the transient dispersion with a crossflow and one-side wall adsorption by calculating the first five moments, and no limit is posed on the adsorption rate. The vertical concentration distribution, remaining mass, effective velocity, dispersivity, and non-Gaussian quantities skewness and kurtosis are accurately derived to cover the preasymptotic process. In addition, the longitudinal distribution of the vertical average concentration and the two-dimensional concentration field is approximated by Chatwin's [26] long-time asymptotic expansion (Edgeworth expansion). The remainder of this paper is organized as follows: The advection-diffusion equation for the concentration and the successive equations for the concentration moments, along with the boundary and initial conditions, are illustrated in Sec. II; in Sec. III, the eigenfunction expansion of moments and the determination of the expansion coefficients are introduced; the results and discussion are given in Sec. IV; a brief conclusion is given in Sec. V; the details of the solution to the eigenvalue problem are presented in Appendix A; in Appendix B, a typical case is directly compared with Brownian dynamics (BD) simulation, showing good agreement; and in Appendix C, we present a standard homogenization method for the steady-state dispersion problem, which is almost identical to the GTD method.

II. GOVERNING EQUATIONS

As depicted in Fig. 1, $\boldsymbol{e}_x$ and $\boldsymbol{e}_y$ denote the unit vectors of longitudinal axis x^* and vertical axis y^*, respectively. The velocity field $\boldsymbol{u} = u^*(y^*)\boldsymbol{e}_x + v^*\boldsymbol{e}_y$ of the canonical pressure-driven flow between two parallel plates with a uniform and perpendicular crossflow is given by Batchelor [37]:

$$u^*(y^*) = -\frac{dp^*}{dx^*}\frac{1}{\rho V^*}\left[-y^* + H^*\frac{1-\exp(-V^*y^*/\nu)}{1-\exp(-V^*H^*/\nu)}\right], \tag{1}$$

$$v^* = -V^*, \tag{2}$$

where $u^*(y^*)$ and v^* are the longitudinal and vertical velocity, respectively, with V^* denoting the absolute value of v^*; $-dp^*/dx^*$ is the pressure gradient driving the main flow, ρ and ν are the density and kinematic viscosity of the fluid, and H^* is the channel height.

The solute concentration C^* is governed by the advection-diffusion equation,

$$\frac{\partial C^*}{\partial t^*} + u^*(y^*)\frac{\partial C^*}{\partial x^*} + v^*\frac{\partial C^*}{\partial y^*} = D^*\left(\frac{\partial^2 C^*}{\partial x^{*2}} + \frac{\partial^2 C^*}{\partial y^{*2}}\right), \tag{3}$$

where D^* is the molecular diffusivity.

Following Lin and Shaqfeh [35], the top boundary is set to be nonreactive, i.e., the adsorption rate is zero, whereas the bottom boundary adsorbs the solute at an adsorption rate k^*, thus the boundary conditions are

$$D^*\frac{\partial C^*}{\partial y^*} + V^*C^* = \{k^*C^*, 0\} \quad \text{at } y^* = \{0, H^*\}. \tag{4}$$

Variables are made dimensionless by

$$C = \frac{C^*}{C_c^*}, \quad x = \frac{x^*}{H^*}, \quad y = \frac{y^*}{H^*}, \quad t = \frac{t^* D^*}{H^{*2}},$$
$$\mathrm{Pe}_u = \frac{U^* H^*}{D^*}, \quad \mathrm{Pe}_v = \frac{V^* H^*}{D^*}, \quad \mathrm{Re}_v = \frac{V^* H^*}{\nu}, \quad \mathrm{Sh} = \frac{k^* H^*}{D^*}. \tag{5}$$

Here C_c^* is a characteristic concentration at the initial release to ensure $\int_{-\infty}^{\infty}\int_0^1 C(x, y, 0)dy\,dx = 1$. For example, if the initial release is a uniform line source at $x^* = 0$, i.e., $C^*(x^*, y^*, 0) = Q^*\delta(x^*)$, where Q^* is the total amount of the solute, then C_c^* is numerically equal to Q^*. Pe_u and Pe_v are the Péclet numbers characterizing the strength of the main longitudinal flow and the crossflow, respectively. $U^* = -(dp^*/dx^*)H^{*2}/(12\rho\nu)$ is the vertical average velocity without the crossflow (planar Poiseuille flow). Re_v is a Reynolds number controlling the longitudinal velocity profile and we shall fix $\mathrm{Re}_v = 1$ throughout this work. Sh is the Sherwood number quantifying the adsorption intensity of the bottom boundary.

The dimensionless equation for the solute transport is

$$\frac{\partial C}{\partial t} + \mathrm{Pe}_u u\frac{\partial C}{\partial x} - \mathrm{Pe}_v\frac{\partial C}{\partial y} = \frac{\partial^2 C}{\partial x^2} + \frac{\partial^2 C}{\partial y^2}, \tag{6}$$

where the longitudinal velocity is now given by

$$u(y) = \frac{12}{\mathrm{Re}_v}\left[-y + \frac{1 - \exp(-\mathrm{Re}_v y)}{1 - \exp(-\mathrm{Re}_v)}\right]. \tag{7}$$

Note that

$$\lim_{\mathrm{Re}_v \to 0} u(y) = -6(-1 + y)y, \tag{8}$$

and the mean longitudinal flow velocity is

$$\overline{u} = \frac{6[2\exp(-\mathrm{Re}_v) - \mathrm{Re}_v \coth(\mathrm{Re}_v/2)]}{{\mathrm{Re}_v}^2}, \tag{9}$$

where $\overline{(\cdot)} \triangleq \int_0^1 (\cdot)dy$ denotes the vertical averaging operation.

The boundary conditions become

$$\frac{\partial C}{\partial y} + \mathrm{Pe}_v C = \{\mathrm{Sh}C, 0\} \quad \text{at } y = \{0, 1\}. \tag{10}$$

The longitudinal moments of concentration are defined as [15]

$$C_p \triangleq \int_{-\infty}^{\infty} x^p C(x, y, t)dx, \quad p = 0, 1, \ldots, \tag{11}$$

where p denotes the order. The vertical average moments $\overline{C_p}$, namely, global moments M_p, are subsequently defined as

$$M_p \triangleq \overline{C_p} = \int_0^1 C_p dy. \tag{12}$$

The governing equations for the moment are obtained by applying $\int_{-\infty}^{\infty}(\cdot)dx$ to Eq. (6),

$$\frac{\partial C_p}{\partial t} = p\,\mathrm{Pe}_u\,u\,C_{p-1} + p\,(p-1)\,C_{p-2} + \mathcal{L}C_p, \tag{13}$$

where

$$\mathcal{L}(\cdot) \triangleq \mathrm{Pe}_v \frac{\partial(\cdot)}{\partial y} + \frac{\partial^2(\cdot)}{\partial y^2}, \tag{14}$$

and we have assumed that the concentration and its longitudinal derivatives decay exponentially as $|x| \to \infty$ [15],

$$C(x, y, t) \to 0 \quad \text{as } x \to \pm\infty, \tag{15}$$

$$\frac{\partial^p C(x, y, t)}{\partial x^p} \to 0 \quad \text{as } x \to \pm\infty, \ p = 1, 2, 3, \ldots \tag{16}$$

to simplify the moment equations.

The corresponding boundary conditions for C_p are

$$\frac{\partial C_p}{\partial y} + \mathrm{Pe}_v C_p = \{\mathrm{Sh} C_p, 0\} \quad \text{at } y = \{0, 1\}. \tag{17}$$

We consider a slug released at $x = 0$, thus the initial condition is formally specified as

$$C(x, y, 0) = \delta(x) f_{\mathrm{ini}}(y), \tag{18}$$

$$C_0(y, 0) = f_{\mathrm{ini}}(y), \tag{19}$$

$$C_p = 0, \quad p = 1, 2, \ldots . \tag{20}$$

Throughout this work, we use vertical uniform release as the initial condition, thus $f_{\mathrm{ini}} = 1$.

III. SOLUTIONS FOR MOMENTS

A. Eigenfunction expansion of moments

We follow Barton [16] to express the moments by eigenfunction expansion,

$$C_p(y, t) = \sum_{i=0}^{\infty} p_{ni}(t) e^{-\lambda_i t} f_i(y), \quad p = 0, 1, \ldots, \tag{21}$$

where $\{-\lambda_i\}_{i=0}^{\infty}$ are the eigenvalues sorted in descending order, and $\{f_i\}_{i=0}^{\infty}$ are the corresponding orthogonal and normalized eigenfunctions. The details of the eigenvalue problem are given in Appendix A. $\{p_{ni}\}_{i=0}^{\infty}$ are the expansion coefficients to be determined by the initial condition.

B. Determination of the expansion coefficients

Due to the dependence of higher-order moment on lower-order moments, Eq. (13) is solved successively. The expansion coefficients $\{p_{ni}\}_{i=0}^{\infty}$ can be subsequently determined by the initial condition and solutions of lower-order moments (for the zeroth-order moment, only the initial condition is used), using the orthogonality of the eigenfunctions $\{f_i\}_{i=0}^{\infty}$. The detailed calculation of the expansion coefficients $\{p_{ni}\}_{i=0}^{\infty}$ can be referred to in Barton [16], or a recent application to the transient dispersion of active particles [38]. We truncate the expansion (21) to a degree of $N = 40$ and convergence is attained.

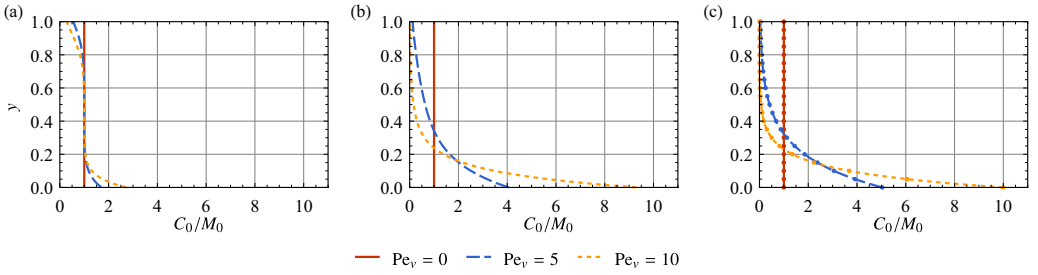

FIG. 2. Temporal evolution of the normalized vertical concentration distribution. $\mathrm{Sh} = 0$ in all cases. $t = \{0.01, 0.1, 1\}$ in (a), (b), and (c), respectively. Vertical concentration distribution at $t = 1$ is compared with distribution at $t = 10$, and they are found to be identical, thus the vertical concentration distribution at $t = 1$ is already steady. Dots with the same color as lines denote the corresponding analytical expression (24) derived by the dual-perturbation method.

IV. RESULTS AND DISCUSSION

A. Zeroth-order moment: Vertical concentration distribution and remaining mass

Assigning $p = 0$ in Eqs. (13) and (17), we obtain the governing equation for the zeroth-order moment C_0 and the corresponding boundary conditions,

$$\frac{\partial C_0}{\partial t} = \mathrm{Pe}_v \frac{\partial C_0}{\partial y} + \frac{\partial^2 C_0}{\partial y^2}, \tag{22}$$

$$\frac{\partial C_0}{\partial y} + \mathrm{Pe}_v C_0 = \{\mathrm{Sh} C_0, 0\} \quad \text{at } y = \{0, 1\}. \tag{23}$$

It is obvious that the solution for C_0 is governed by two dimensionless parameters, namely, the Péclet for the crossflow Pe_v and the Sherwood number Sh.

In Figs. 2 and 3 we show the temporal evolution of the normalized vertical concentration distribution C_0/M_0. The analytical result derived by Lin and Shaqfeh [35] using the dual-perturbation method is also plotted. Their analytical expression in the current notation is

$$\frac{C_0}{M_0} = \mathcal{P}(y) + \mathrm{Sh}\mathcal{P}(y)\mathcal{Q}(y), \tag{24}$$

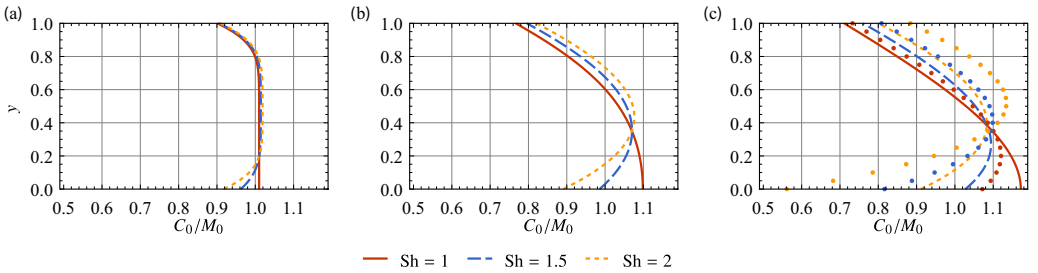

FIG. 3. Temporal evolution of the normalized vertical concentration distribution. $\mathrm{Pe}_v = 1$ in all cases. $t = \{0.01, 0.1, 1\}$ in (a), (b), and (c), respectively. Vertical concentration distribution at $t = 1$ is compared with distribution at $t = 10$, and they are found to be identical, thus the vertical concentration distribution at $t = 1$ is already steady. Dots with the same color as lines denote the corresponding analytical expression (24) derived by the dual-perturbation method.

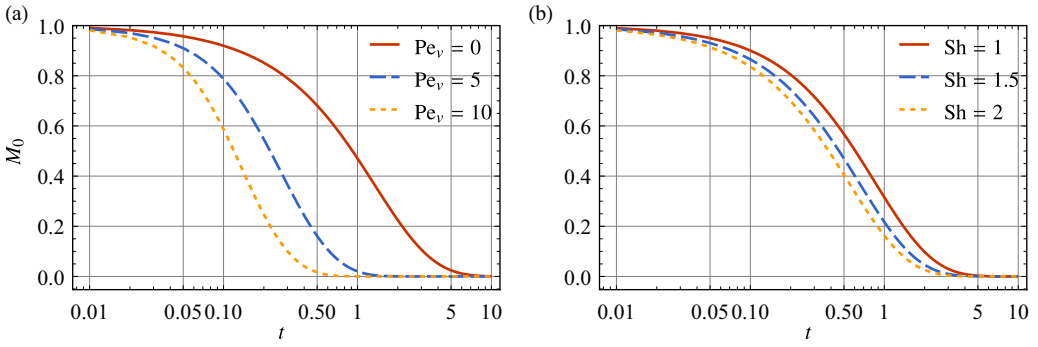

FIG. 4. Temporal evolution of zeroth-order total moment M_0 (remaining mass in the flow domain). $\mathrm{Sh} = 1$ in (a), $\mathrm{Pe}_v = 1$ in (b).

where

$$\mathcal{P}(y) = \mathrm{Pe}_v \frac{\exp(-\mathrm{Pe}_v y)}{1 - \exp(-\mathrm{Pe}_v)}, \tag{25}$$

$$\mathcal{Q}(y) = \frac{\exp(\mathrm{Pe}_v)\mathrm{Pe}_v y - \exp(\mathrm{Pe}_v y) + 1}{[\exp(\mathrm{Pe}_v) - 1]\mathrm{Pe}_v} + \frac{\sinh(\mathrm{Pe}_v) - \mathrm{Pe}_v}{[1 - \cosh(\mathrm{Pe}_v)]\mathrm{Pe}_v}. \tag{26}$$

It should be noted that the original analytical expression derived by Lin and Shaqfeh [35] [Eq. (18) in their paper] was for the concentration C, instead of the zeroth-order longitudinal concentration moment C_0; however, one can take the zeroth-order longitudinal moment $[\int_{-\infty}^{\infty}(\cdot)dx]$ of their analytical expression with the condition that C decays exponentially as $x \to \pm\infty$ [15], and the result is exactly Eq. (24). Built for the asymptotic state, Eq. (24) was also used by Lin and Shaqfeh [35] as the vertical concentration distribution at the Gaussian center of the solute patch.

In Fig. 2, we see that the concentration at the bottom boundary increases with t and Pe_v. This result is due to the crossflow pushing the solute to the bottom boundary. When $t = 1$, C_0/M_0 has equilibrated and good agreement is seen between the results obtained with moments and the analytical expression (24). It is noted that, when both boundaries are nonreactive, i.e., $\mathrm{Sh} = 0$, $\mathcal{P}(y)$ given in Eq. (25) is the vertical concentration distribution. Additionally, if $\mathrm{Sh} = 0$, one can also drop the time derivative in Eq. (22) and solve the steady vertical concentration distribution with the corresponding boundary conditions, and the result is consistent with Eq. (25).

The evolution of C_0/M_0 with $\mathrm{Sh} \neq 0$ is plotted in Fig. 3. We see that the concentration near the top boundary decreases with t, due to the crossflow, whereas the variation of concentration near the bottom boundary depends on the adsorption rate Sh: with a smaller Sh, for example, $\mathrm{Sh} = 1$, the concentration near the bottom boundary is the highest and increases with t; in contrast, with a larger Sh, for example, $\mathrm{Sh} = 2$, the concentration near the bottom boundary decreases with t due to high adsorption. For the comparison with analytical expression (24), we see in Fig. 3(c) that Eq. (24) is inaccurate for a relatively large Sh as a consequence of Sh being an expansion quantity assumed to be small in the dual-perturbation method.

The evolution of remaining mass M_0 in the flow domain is plotted in Fig. 4. As expected, both a stronger crossflow and a larger adsorption rate can largely enhance the effective adsorption. It is understood by considering the effective mass-transfer rate

$$\frac{dM_0}{dt} = \mathrm{Sh} C_0(0, t). \tag{27}$$

For the initial and intermediate stages, if Pe_v is increased, $C_0(0, t)$ increases and finally leads to the increase of dM_0/dt. If Sh is increased, dM_0/dt still increases even though $C_0(0, t)$ may decrease.

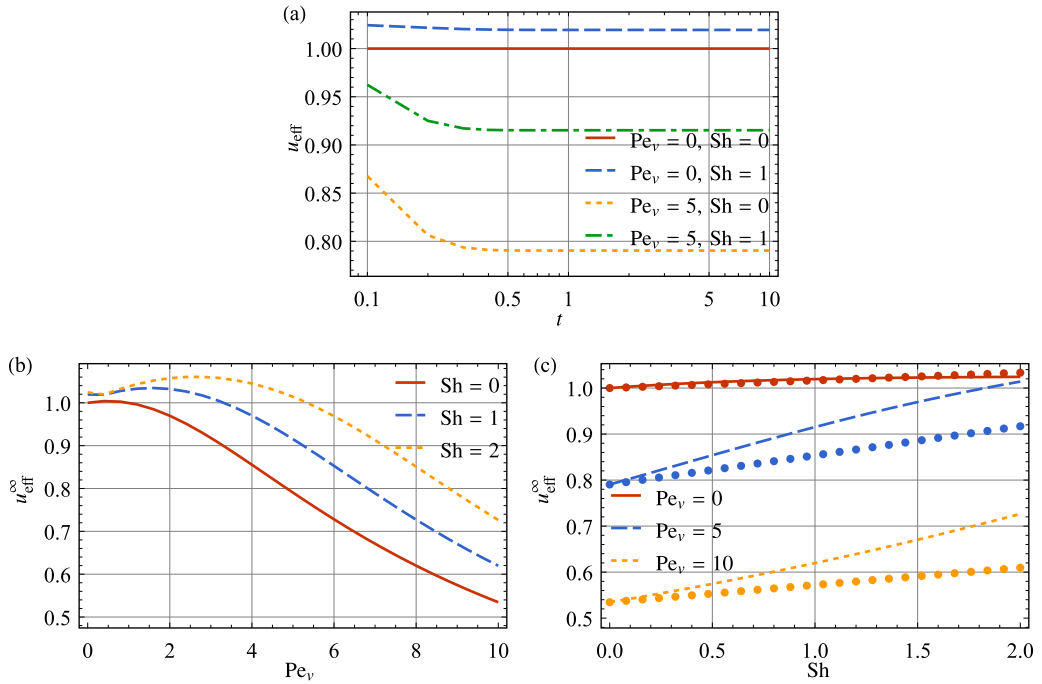

FIG. 5. (a) Temporal evolution of effective velocity u_{eff}; (b) steady effective velocity u^{∞}_{eff} as a function of the Péclet number for the crossflow Pe_v; and (c) steady effective velocity u^{∞}_{eff} as a function of the Sherwood number Sh; dots denote results of Lin and Shaqfeh [35]. $\text{Pe}_u = 100$ in all cases.

For the long-time stage, the effective mass-transfer rates of cases with large Pe_v and Sh approach zero earlier, due to low $C_0(0, t)$ at this stage.

B. First-order moment: Effective velocity

The effective velocity describes the average longitudinal velocity of the substance in the flow domain, and is defined as

$$u_{\text{eff}} = \frac{1}{\text{Pe}_u \overline{u}} \frac{d\overline{\mu}}{dt}, \tag{28}$$

where

$$\overline{\mu} = \frac{M_1}{M_0} \tag{29}$$

is mass center of the solute. Care should be taken that u_{eff} does not coincide with the ratio of vertical average longitudinal velocity of the substance in the flow domain $\int_0^1 (C_0/M_0) u \, dy$ to the mean flow $\text{Pe}_u \overline{u}$, in contrast to dispersion with conserved total mass ($M_0 = 1$). This difference is because the substance near the bottom is more likely to be adsorbed and has less contribution to the effective velocity [see, e.g., Eq. (C20) in Appendix C].

As shown in Fig. 5, if the bottom boundary is adsorbable (Sh > 0) and no crossflow is supplied ($\text{Pe}_v = 0$), both u_{eff} and u^{∞}_{eff} are greater than 1, demonstrating that the solute moves faster on average than the mean flow. This result is attributed to the diminution of solute concentration at the bottom where the local flow is slow. In contrast, if a crossflow is supplied ($\text{Pe}_v > 0$), both u_{eff} and u^{∞}_{eff} can be possibly smaller than 1, as a consequence of concentrated solute at the low-speed bottom region. For example, in Fig. 5(b) we see that $u^{\infty}_{\text{eff}} < 1$ for all cases provided that Pe_v is sufficiently

large. In addition, when $\mathrm{Sh} \neq 0$, $u_{\mathrm{eff}}^{\infty}$ exhibits a complex nonmonotonic variation as a function of Pe_v. As shown in Fig. 5(b), for a nonzero Sh, $u_{\mathrm{eff}}^{\infty}$ notably first increases and then decreases with increasing Pe_v. This result can be understood by considering the following reasoning: when Pe_v is relatively small to Sh, the crossflow pushes the substance to the middle-bottom region and the adsorbable boundary further decreases the concentration at the boundary, therefore the normalized vertical concentration distribution is peaked at the high-speed central region [see, e.g., Fig. 3(c) with $\mathrm{Sh} = 2$], and thus $u_{\mathrm{eff}}^{\infty}$ is increased; when Pe_v is relatively large to Sh, the adsorbable boundary is unable to consume the high concentration at the bottom, and the normalized vertical concentration distribution is peaked at the low-speed bottom region [see, e.g., Fig. 3(c) with $\mathrm{Sh} = 1$], and thus $u_{\mathrm{eff}}^{\infty}$ is decreased.

In Fig. 5(c), we see that the variation of $u_{\mathrm{eff}}^{\infty}$ as a function of Sh is monotonic: by removing substance at the bottom low-speed region, an increasing Sh enhances $u_{\mathrm{eff}}^{\infty}$, especially in the presence of a crossflow. This result is directly reflected in the effect of Sh on the normalized vertical concentration distribution (see, e.g., Fig. 3). The dual-perturbation result of Lin and Shaqfeh [35], however, underestimates the effect of Sh on $u_{\mathrm{eff}}^{\infty}$ when a crossflow is present. Moreover, we see that the results of the dual-perturbation method deviate from the current as Sh increases due to the restriction on adsorption rate.

C. Second-order moment: Dispersivity

The dispersivity is defined as

$$D_{\mathrm{T}} = \frac{1}{2}\frac{d\overline{\sigma}^2}{dt}, \tag{30}$$

where

$$\overline{\sigma}^2 = \frac{M_2}{M_0} - \overline{\mu}^2 \tag{31}$$

is the variance of the vertical average concentration $\overline{C}$. The dispersivity D_{T} characterizes the longitudinal dispersion process, and its long-time limit D_{T}^{∞} is the Taylor dispersivity.

The temporal evolution of D_{T} and the variations of D_{T}^{∞} as functions of Pe_u, Pe_v, and Sh are plotted in Fig. 6. For the temporal evolution, D_{T} is seen to increase with time and reach the steady state. However, the time when the steady state of D_{T} is reached obviously varies with the following cases: when $(\mathrm{Pe}_v, \mathrm{Sh}) = (5, 1)$, the corresponding time is $t \sim 0.5$, whereas the corresponding times for $(\mathrm{Pe}_v, \mathrm{Sh}) = (0, 0)$ and $(\mathrm{Pe}_v, \mathrm{Sh}) = (5, 0)$ are $t \sim 0.2$ and $t \sim 0.1$, respectively. This result suggests a delayed time to enter the steady dispersion regime for case with a crossflow and wall adsorption; however, this important pre-asymptotic dispersion regime is seldom discussed in previous works.

With increasing Pe_u, D_{T}^{∞} increases monotonically, and $D_{\mathrm{T}}^{\infty} \sim \mathrm{Pe}_u^2$ at large Pe_u, as indicated in Fig. 6(b) and consistent with previous works. The variation of D_{T}^{∞} as a function of Pe_v is rather complex. While D_{T}^{∞} exhibiting a monotonic decrease for asymptotically large Pe_v can be easily understood by recognizing that a concentration boundary layer is developed at the bottom, the variation before this limit is difficult to inspect with intuition. A similar complex variation of D_{T}^{∞} as a function of Sh is also observed, as shown in Fig. 6(d). Although an increasing Sh leads to a depleted concentration at the bottom, whether this effect enhances or weakens dispersion depends on the strength of the crossflow: when Pe_v is small (e.g., $\mathrm{Pe}_v = 0$), Sh almost does not influence dispersion; when Pe_v is large (e.g., $\mathrm{Pe}_v = 10$), dispersion increases with Sh due to the destruction of the concentration boundary layer; when Pe_v is moderate (e.g., $\mathrm{Pe}_v = 5$), an increasing Sh first enhances dispersion by removing the concentration boundary layer and then weakens dispersion by excessively removing the substance at the high-shear bottom region. We note that due to the restriction of the dual-perturbation method to a weak adsorption rate, its result cannot reflect the effect of Sh on D_T^{∞}, as depicted in Fig. 6(d).

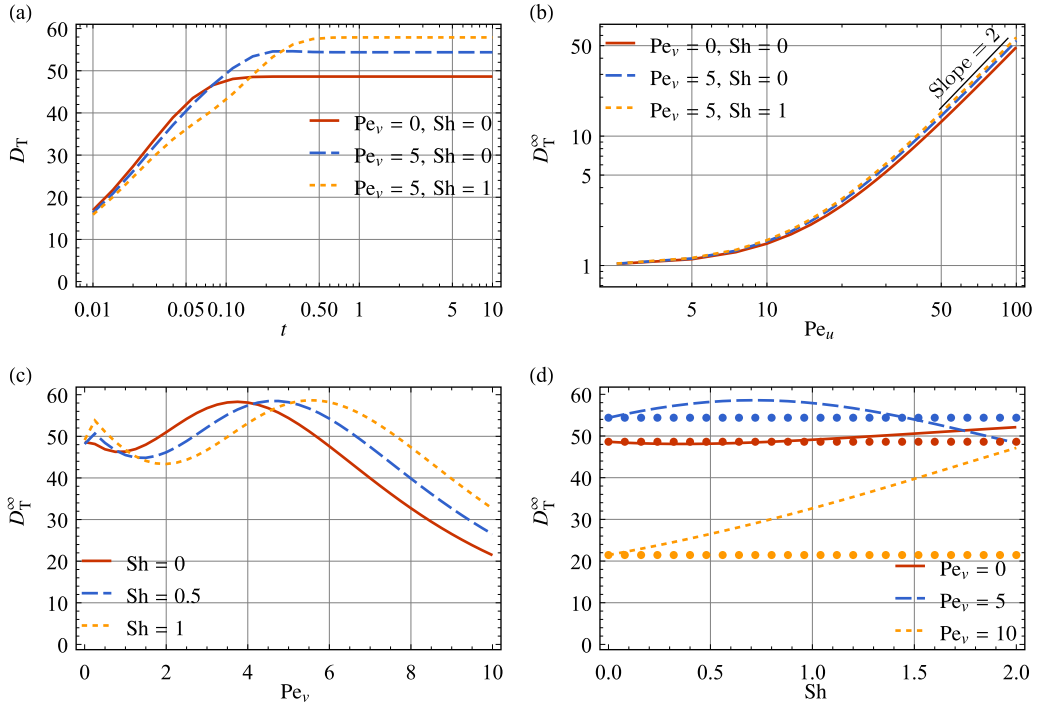

FIG. 6. (a) Temporal evolution of dispersivity D_T; (b) steady dispersivity D_T^∞ as a function of the Péclet number for the main flow Pe_u; (c) steady dispersivity D_T^∞ as a function of the Péclet number for the crossflow Pe_v; and (d) steady dispersivity D_T^∞ as a function of the Sherwood Sh; dots denote the results of Lin and Shaqfeh [35]. $\mathrm{Pe}_u = 100$ in (a), (c), and (d).

D. Higher-order moments: Skewness, kurtosis, and concentration

The global skewness $\overline{\gamma_1}$ and kurtosis $\overline{\gamma_2}$ are defined as

$$\overline{\gamma_1} = \frac{\overline{\kappa_3}}{\overline{\sigma}^3}, \tag{32}$$

$$\overline{\gamma_2} = \frac{\overline{\kappa_4}}{\overline{\sigma}^4}, \tag{33}$$

where $\overline{\kappa_3}$ and $\overline{\kappa_4}$ are the third and fourth global cumulants defined as

$$\overline{\kappa_3} = \frac{M_3}{M_0} - 3\overline{\mu}\,\overline{\sigma}^2 - \overline{\mu}^3, \tag{34}$$

$$\overline{\kappa_4} = \frac{M_4}{M_0} - 4\overline{\mu}\frac{M_3}{M_0} + 6\overline{\mu}^2\overline{\sigma}^2 + 3\overline{\mu}^3 - 2\overline{\sigma}^4. \tag{35}$$

We use fourth-order Edgeworth expansion of the moments to approximate the longitudinal distribution of the vertical average concentration and two-dimensional concentration field. The fourth-order Edgeworth expansion for the two-dimensional concentration field is

$$C(X,y,t) \sim C_0 \frac{\exp(-X^2/2)}{\sqrt{2\pi}\sigma}\left\{1 + \left[\frac{\kappa_3}{3!\sigma^3}He_3(X)\right] + \left[\frac{\kappa_4}{4!\sigma^4}He_4(X) + \frac{10\kappa_3^2}{6!\sigma^6}He_6(X)\right]\right\}, \tag{36}$$

where

$$X = \frac{x-\mu}{\sigma} \tag{37}$$

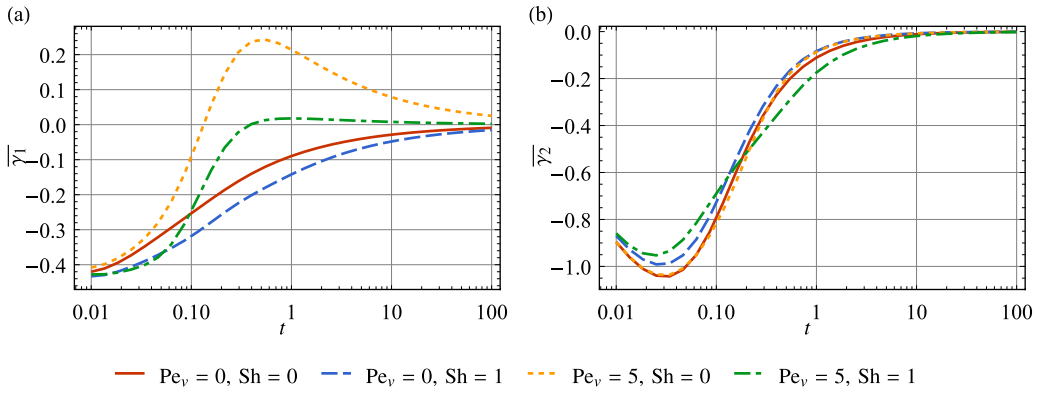

FIG. 7. Temporal evolution of skewness $\overline{\gamma}_1$ (a) and kurtosis $\overline{\gamma}_2$ (b). $\mathrm{Pe}_u = 100$ in all cases.

is the rescaled longitudinal coordinate. In addition, μ, σ, κ_3, and κ_4 are now evaluated with local moments C_p instead of global moments M_p in Eqs. (29), (31), and (35). To approximate the vertical average concentration $\overline{C}$, one can directly use

$$\overline{C}(X,t) \sim \overline{C}_0 \frac{\exp(-X^2/2)}{\sqrt{2\pi}\overline{\sigma}} \left\{ 1 + \left[\frac{\overline{\kappa_3}}{3!\overline{\sigma}^3} He_3(X) \right] + \left[\frac{\overline{\kappa_4}}{4!\overline{\sigma}^4} He_4(X) + \frac{10\overline{\kappa_3}^2}{6!\overline{\sigma}^6} He_6(X) \right] \right\}. \tag{38}$$

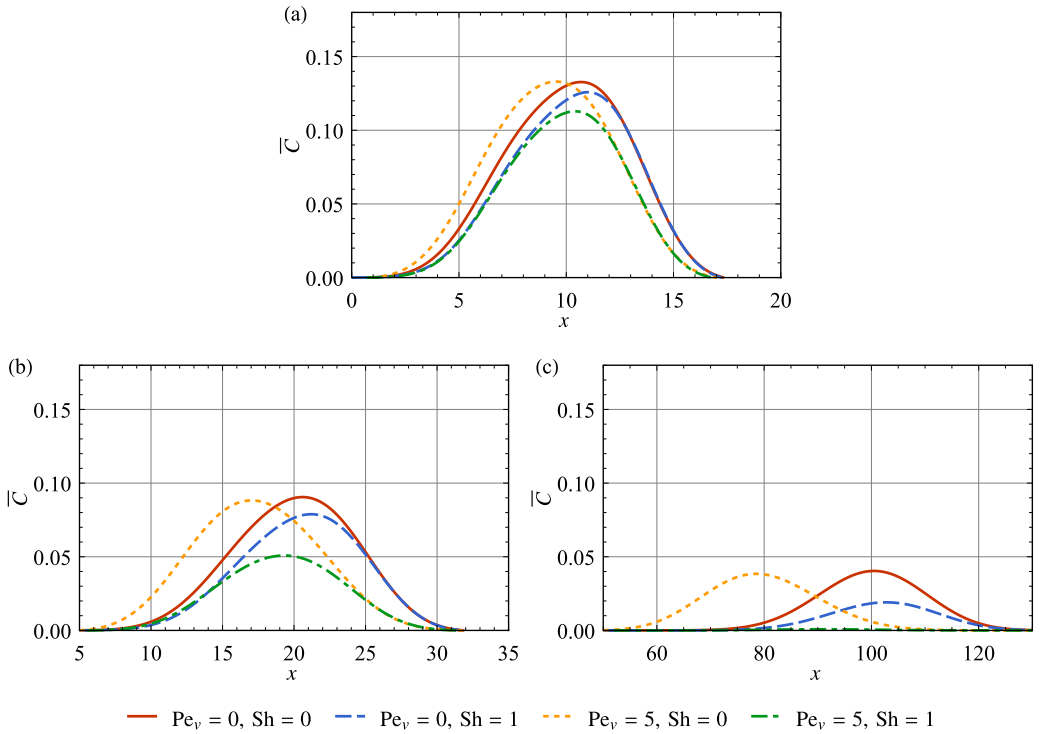

FIG. 8. Temporal evolution of the longitudinal distribution of vertical average concentration $\overline{C}$ obtained with Edgeworth expansion. $t = \{0.1, 0.2, 1\}$ in (a), (b), and (c), respectively. $\mathrm{Pe}_u = 100$ in all cases.

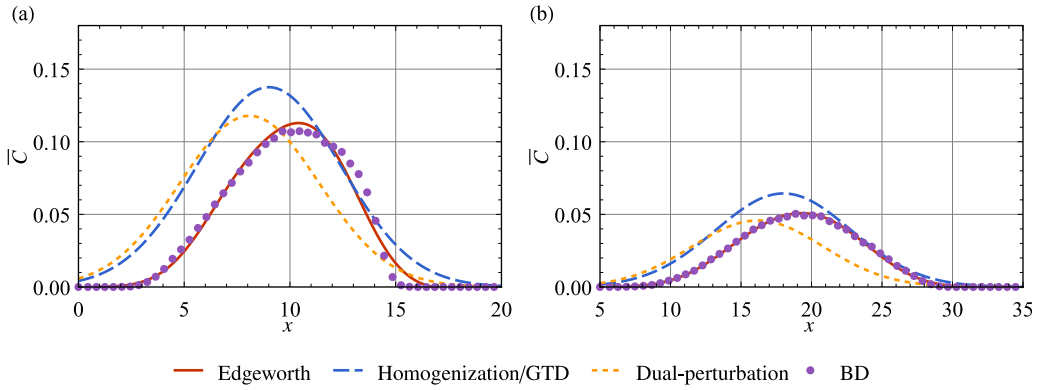

FIG. 9. Comparison of longitudinal distribution of vertical average concentration $\overline{C}$ obtained from Edgeworth expansion with moments, the homogenization/GTD method, the dual-perturbation method of Lin and Shaqfeh [35], and BD simulations. $t = \{0.1, 0.2\}$ in (a) and (b), respectively. $\mathrm{Pe}_u = 100$, $\mathrm{Re}_v = 1$, $\mathrm{Pe}_v = 5$, and $\mathrm{Sh} = 1$.

We note that the Edgeworth expansion can be derived from an asymptotic expansion for C as shown by Chatwin [26]. In addition, from a statistic view, it can be understood as an expansion for a nearly Gaussian distribution [39], since C at each streamline and its vertical average $\overline{C}$ gradually tend to Gaussian [26,40,41].

Skewness $\overline{\gamma_1}$ and kurtosis $\overline{\gamma_2}$ quantify the asymmetry and deviation from Gaussian distribution, respectively. As shown in Fig. 7(a), although the skewness $\overline{\gamma_1}$ in all cases approach zero asymptotically, their evolution can be significantly different. While other cases almost exhibit negative skewness as they are evolving to the steady dispersion regime, the case with solely a crossflow $(\mathrm{Pe}_v, \mathrm{Sh}) = (5, 0)$ exhibits positive skewness at the moderate time ($t \sim 0.5$). Positive skewness is understood by a downstream tail of the longitudinal concentration distribution, and negative skewness is the opposite. We further plot the longitudinal distribution of vertical average concentration in Fig. 8 for $t = \{0.2, 1, 1\}$, and the downstream tail of the case with $(\mathrm{Pe}_v, \mathrm{Sh}) = (5, 0)$ is observed, whereas other cases have upstream tails. In contrast to skewness, the evolution of kurtosis $\overline{\gamma_2}$ of the four cases are similar. As shown in Fig. 7, $\overline{\gamma_2}$ of all cases first decrease and then increase and finally approach zero, demonstrating that longitudinal Gaussian distribution is attained eventually.

In Fig. 9 we further plot the comparison of longitudinal distribution of vertical average concentration $\overline{C}$ obtained from Edgeworth expansion (38), the dual-perturbation method of Lin and Shaqfeh [35, Eq. (9)], the GTD method [36,42] [see also Eq. (C27)], and the Brownian dynamics simulations (see Appendix B). Good agreement is seen between the results of Edgeworth expansion and BD simulations. Although GTD gives an acceptable downstream concentration distribution, both GTD and the dual-perturbation method underperform in the upstream region, and predict inaccurate values and slower advection velocities of the maximum concentration.

The approximate two-dimensional concentration field is plotted in Fig. 10. By comparing different cases, we see that while a crossflow pushes the concentration towards the bottom boundary obviously, the adsorption at the bottom boundary only weakens the concentration slightly. The crossflow results in a maximum concentration at the bottom. By adsorbing the substance, the adsorbable bottom boundary weakens the concentration, especially in the presence of a crossflow.

V. CONCLUSIONS

Using the classical method of moments solved by separation of variables, we have presented a detailed analysis of the dispersion process in a channel flow with a crossflow and with only the bottom boundary being adsorbable. Although this configuration has been investigated previously, the

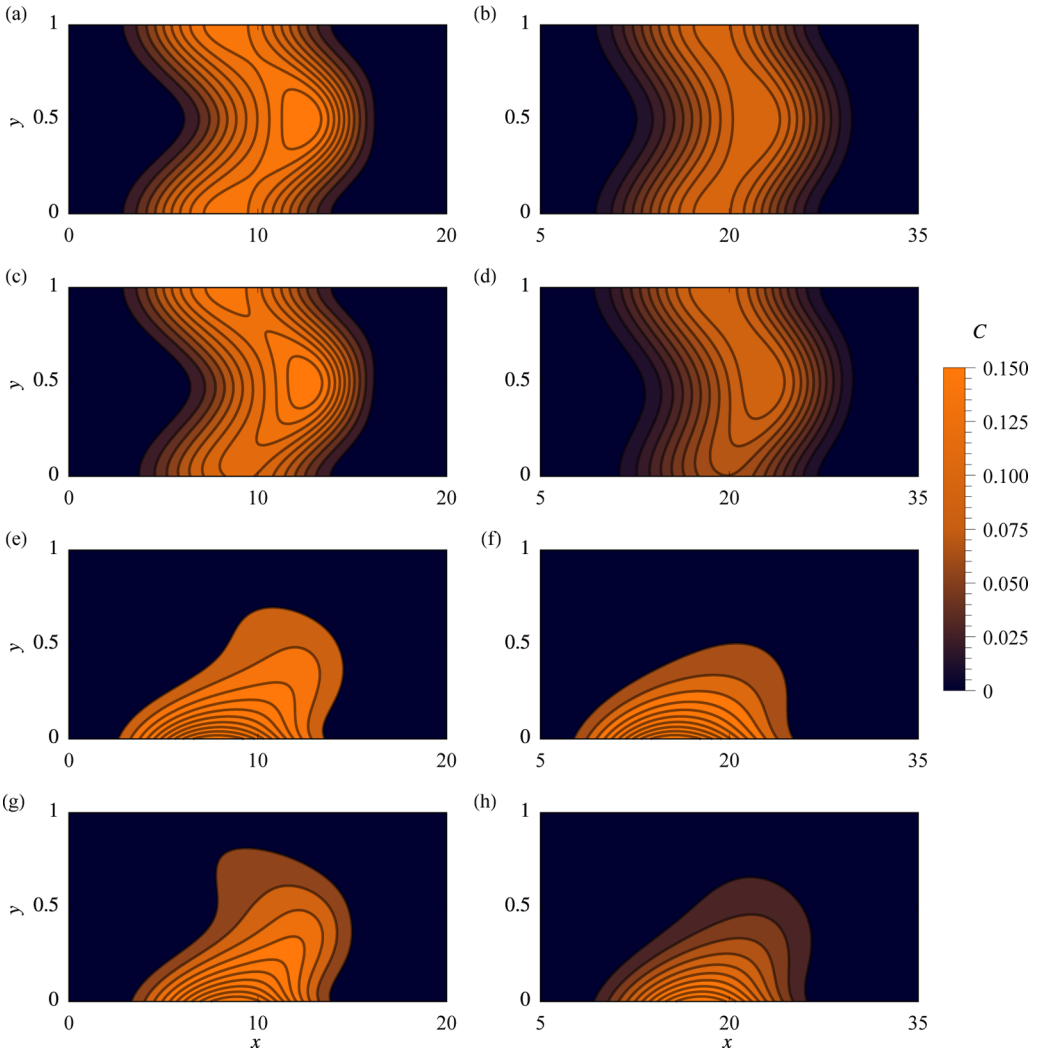

FIG. 10. Temporal evolution of the two-dimensional concentration distribution C obtained with Edgeworth expansion. $t = \{0.1, 0.2\}$ in (a), (c), (e), (g) and (b), (d), (f), (h), respectively. (a), (b) $\mathrm{Pe}_v = 0$, $\mathrm{Sh} = 0$; (c), (d) $\mathrm{Pe}_v = 0$, $\mathrm{Sh} = 1$; (e), (f) $\mathrm{Pe}_v = 5$, $\mathrm{Sh} = 0$; and (g), (h) $\mathrm{Pe}_v = 5$, $\mathrm{Sh} = 1$. and $\mathrm{Pe}_u = 100$ in all cases.

current work discussed the preasymptotic dispersion regime by calculating the moments up to fourth order. The dispersion coefficients of Shapiro and Brenner [36] are asymptotically accurate, because they used the GTD method by keeping the largest negative eigenvalue $-\lambda_0$ in Eq. (21), which is dominant at the long-time asymptotic state. Nonetheless, the asymptotic dispersion coefficients are far from enough to describe the transient dispersion process. We have now shown the strong non-Gaussian properties in the preasymptotic dispersion regime and how the dispersion coefficients evolve with time. Aiming also at the asymptotic dispersion regime, another related work by Lin and Shaqfeh [35] using the dual-perturbation method, is however restricted to a weak adsorption rate.

While both a larger Sh and Pe_v enhance the effective mass transfer, the vertical concentration distribution is influenced by the competing strengths of Sh and Pe_v, which can lead to a maximum concentration at the bottom or the middle. The variation of vertical concentration distribution further complicates higher-order dispersion coefficients, as reflected by the nonmonotonic variations of

the dispersion coefficients as functions of Sh and Pe_v. For the transient dispersion process, we have given both the accurate temporal dispersion coefficients and the approximated longitudinal and two-dimensional concentration distribution using the information contained in higher-order moments, and good agreement with BD simulations is demonstrated. It is important to note that, while the works of Shapiro and Brenner [36] and Lin and Shaqfeh [35] aimed at the asymptotic dispersion regime with a corresponding dimensionless time $t \sim 1$, there is a very small amount of remaining mass in the flow domain at that time. Therefore, although using the asymptotic dispersion coefficients may perform well in cases with conserved mass, it is insufficient to investigate such a case with boundary adsorption.

The current work can be easily extended to some relevant applications, such as nonuniform vertical drift speed and diffusivity [35], as well as dispersion of fine sediment in a turbulent open-channel flow with the deposition rate at the bottom specified. In addition, with the moments accurately solved, one can also employ Gill's generalized dispersion model [17], which was initially proposed for reactive dispersion problems.

ACKNOWLEDGMENTS

This work is supported by the National Natural Science Foundation of China (Grants No. 52079001, No. 52109093, and No. 51879002). W.J. acknowledges the support of China Postdoctoral Science Foundation (Grant No. 2021M701906) and the Shuimu Tsinghua Scholar Program.

APPENDIX A: THE EIGENVALUE PROBLEM

The eigenvalue problem associated with the operator $\mathcal{L}$ (14) is

$$\mathcal{L}f \triangleq \frac{\partial^2 f}{\partial y^2} + \mathrm{Pe}_v \frac{\partial f}{\partial y} = -\lambda f, \tag{A1}$$

with the boundary conditions

$$\frac{\partial f}{\partial y} + \mathrm{Pe}_v f = \{\mathrm{Sh} f, 0\}, \quad \text{at } y = \{0, 1\}. \tag{A2}$$

We rewrite the eigenvalue problem in a standard Sturm-Liouville form

$$\mathcal{L}_s f = -\lambda e^{\mathrm{Pe}_v y} f, \tag{A3}$$

where the self-adjoint operator $\mathcal{L}_s$ is defined as

$$\mathcal{L}_s(\cdot) \triangleq \frac{d}{dy}\left[w(y)\frac{d(\cdot)}{dy}\right] = w(y)\mathcal{L}(\cdot), \tag{A4}$$

where the weighting function is found to be

$$w(y) = e^{\mathrm{Pe}_v y}. \tag{A5}$$

The roots of the auxiliary equation of Eq. (A1) are

$$r_1 = -\frac{\mathrm{Pe}_v}{2} + \frac{1}{2}\sqrt{\mathrm{Pe}_v^2 - 4\lambda}, \quad r_2 = -\frac{\mathrm{Pe}_v}{2} - \frac{1}{2}\sqrt{\mathrm{Pe}_v^2 - 4\lambda}. \tag{A6}$$

The classification of the roots (A6) is discussed as follows.

If $r_1 = r_2$, then $\lambda = \mathrm{Pe}_v^2/4$. The only nontrivial possible eigenfunction

$$f(y) = a_1\left(1 - \frac{\mathrm{Pe}_v}{\mathrm{Pe}_v + 2}y\right)e^{-(\mathrm{Pe}_v/2)y} \tag{A7}$$

exists when

$$\mathrm{Sh} = \frac{\mathrm{Pe}_v^2}{2\mathrm{Pe}_v + 4}, \tag{A8}$$

where a_1 is a constant for normalization.

If $r_1 \neq r_2$, and $0 \leqslant \lambda < \mathrm{Pe}_v^2/4$, the eigenfunctions are

$$f(y) = a_2 e^{-(\mathrm{Pe}_v/2)y}[(\mathrm{Pe}_v - 2\mathrm{Sh})\sinh(\alpha y) - 2\alpha\cosh(\alpha y)], \tag{A9}$$

with the eigenvalues determined by the transcendental equation

$$\left(\tfrac{1}{4}\mathrm{Pe}_v^2 - \tfrac{1}{2}\mathrm{Pe}_v\mathrm{Sh} - \alpha^2\right)\tanh\alpha - \alpha\mathrm{Sh} = 0, \tag{A10}$$

where $\alpha = \sqrt{\mathrm{Pe}_v^2/4 - \lambda}$ and a_2 is a constant for normalization.

If $r_1 \neq r_2$, and $\lambda > \mathrm{Pe}_v^2/4$, the eigenfunctions are

$$f(y) = a_3 e^{-(\mathrm{Pe}_v/2)y}[2\beta\cos(\beta y) + (2\mathrm{Sh} - \mathrm{Pe}_v)\sin(\beta y)] \tag{A11}$$

with the eigenvalues determined by the transcendental equation

$$\mathrm{Sh}\beta\cos\beta + \tfrac{1}{2}\mathrm{ShPe}_v\sin\beta - \tfrac{1}{4}\mathrm{Pe}_v^2\sin\beta - \beta^2\sin\beta = 0, \tag{A12}$$

where $\beta = \sqrt{\lambda - \mathrm{Pe}_v^2/4}$ and a_3 is a constant for normalization.

All eigenvalues are sorted in a descending order $\{-\lambda_i\}_{i=0}^N$, with the corresponding eigenfunctions denoted by $\{f_i(y)\}_{i=0}^N$. Note that the eigenvalue problem was partially solved by Shapiro and Brenner [36]; however, the GTD method they used only retains the largest negative eigenvalue $-\lambda_0$ and the corresponding eigenfunction $f_0(y)$, as shown in Appendix C.

APPENDIX B: BROWNIAN DYNAMICS SIMULATION

BD simulations are performed to validate the moments-based results. The stochastic differential equations of Eq. (6) are

$$dx = \mathrm{Pe}_u u(y)dt + \sqrt{2}dW_x, \tag{B1}$$

$$dy = -\mathrm{Pe}_v dt + \sqrt{2}dW_y, \tag{B2}$$

where dW_x and dW_y are independent Gaussian random numbers with common mean 0 and variance dt.

In the simulation, following Lin and Shaqfeh [35], we use the Euler-Maruyama scheme and a small time step $\Delta t = 10^{-5}$ to accurately capture the adsorbable boundary. A total number of 10^6 solute particles are simulated. The solute particle is reflected back at the top nonadsorbable boundary, while it can escape the flow domain with a probability $\mathrm{Sh}\sqrt{\pi dt}$ at the bottom adsorbable boundary or otherwise performs reflection. Readers are referred to Refs. [43,44] for the details of the equivalence between the treatment at the adsorbable boundary and the continuum boundary condition when the Euler-Maruyama forward scheme is adopted.

The validation of the method of moments against Brownian dynamics simulation is plotted in Fig. 11, demonstrating good agreement. The comparison of the two-dimensional concentration field approximated by Edgeworth expansion and BD simulations is plotted in Fig. 12 and good performance of Edgeworth expansion is seen.

APPENDIX C: A STANDARD HOMOGENIZATION METHOD (GTD METHOD)

In this Appendix we present a standard homogenization method for the long-time asymptotic dispersion problem [45–47]. We also note that this homogenization method is essentially identical to the GTD method [36,42], as pointed out by Rubinstein and Mauri [48].

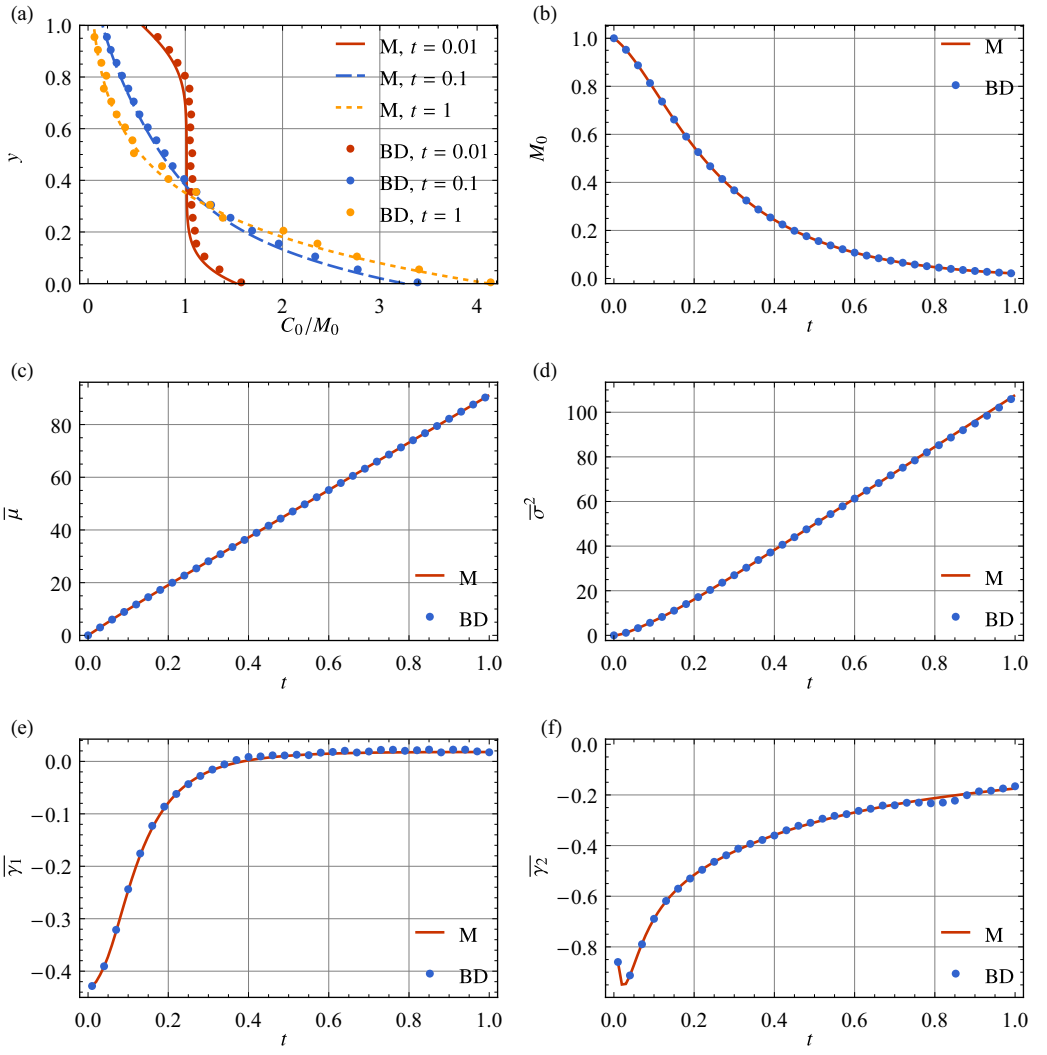

FIG. 11. Validation of the method of moments against Brownian dynamics simulation. "M" and "BD" denote the results of method of moments and Brownian dynamics simulation, respectively. $\mathrm{Pe}_u = 100$, $\mathrm{Pe}_v = 5$, and $\mathrm{Sh} = 1$ in all cases.

The concentration C is decomposed as

$$C(x, y, t) = \mathrm{e}^{-\lambda_0 t}\tilde{C}(x, y, t), \tag{C1}$$

where $-\lambda_0$ is the largest negative eigenvalue determined in Appendix A (or can be referred to as effective reaction rate). Equation (C1) enables $\tilde{C}$ to be a conserved quantity at the long-time asymptotic state [36,42,45]..

Inserting Eq. (C1) into Eqs. (6) and (10), one obtains

$$\frac{\partial \tilde{C}}{\partial t} + \mathrm{Pe}_u u\frac{\partial \tilde{C}}{\partial x} - \frac{\partial^2 \tilde{C}}{\partial x^2} = \lambda_0 \tilde{C} + \mathcal{L}\tilde{C} \tag{C2}$$

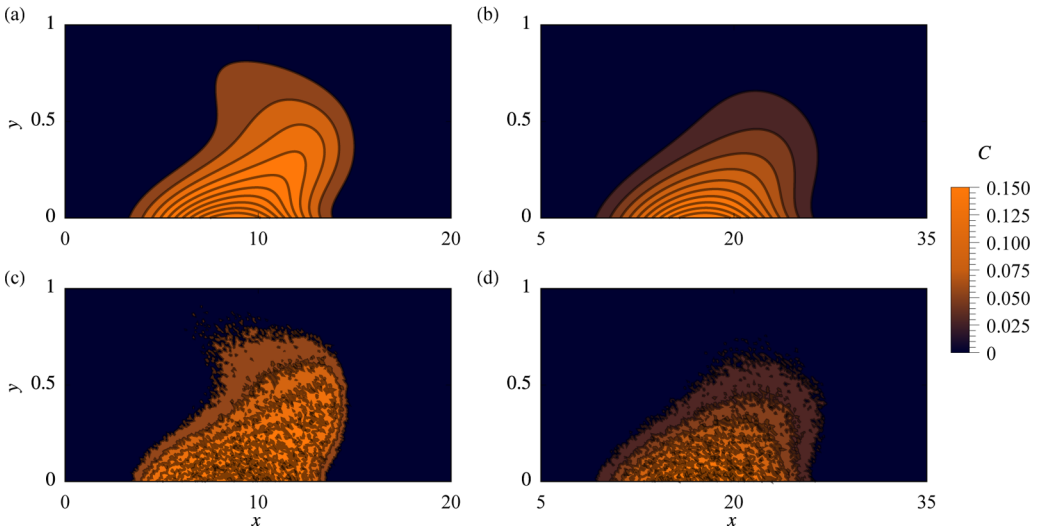

FIG. 12. Comparison of the two-dimensional concentration field approximated by Edgeworth expansion and BD simulations. $t = \{0.1, 0.2\}$ in (a), (c) and (b), (d), respectively. (a), (b) Edgeworth expansion and (c), (d) BD simulation. $\mathrm{Pe}_u = 100$, $\mathrm{Pe}_v = 5$, and $\mathrm{Sh} = 1$ in all cases.

and

$$\frac{\partial \tilde{C}}{\partial y} + \mathrm{Pe}_v \tilde{C} = \{\mathrm{Sh}\tilde{C}, 0\} \quad \text{at } y = \{0, 1\}. \tag{C3}$$

A reference frame moving with the mass center of the substance patch is used to see the pure diffusive behavior; the new reference frame is $x \to x - \mathrm{Pe}_u \bar{u} u_{\mathrm{eff}}^{\infty} t$, thus Eq. (C2) becomes

$$\frac{\partial \tilde{C}}{\partial t} + u_x \frac{\partial \tilde{C}}{\partial x} - \frac{\partial^2 \tilde{C}}{\partial x^2} = \mathcal{L}_c \tilde{C}, \tag{C4}$$

where

$$u_x = \mathrm{Pe}_u u - \mathrm{Pe}_u \bar{u} u_{\mathrm{eff}}^{\infty}, \tag{C5}$$

$$\mathcal{L}_c(\cdot) \triangleq \mathcal{L}(\cdot) + \lambda_0(\cdot). \tag{C6}$$

The typical diffusive scaling [45–47]

$$x = \epsilon \xi, \quad t = \epsilon^{-2} \tau \tag{C7}$$

is used to rescale the transport equation. Here ϵ is a small parameter, and can be understood by H^*/L^*, where L^* is the characteristic length of the substance spreading. The rescaled transport equation becomes

$$\epsilon^2 \frac{\partial \tilde{C}}{\partial \tau} + \epsilon u_x \frac{\partial \tilde{C}}{\partial \xi} - \epsilon^2 \frac{\partial^2 \tilde{C}}{\partial \xi^2} = \mathcal{L}_c \tilde{C}. \tag{C8}$$

$\tilde{C}$ is expanded in a standard perturbation series

$$\tilde{C} = \tilde{C}_0 + \epsilon \tilde{C}_1 + \epsilon^2 \tilde{C}_2. \tag{C9}$$

Inserting Eq. (C9) into Eq. (C8), the problems at successive orders $O(1)$, $O(\epsilon)$, and $O(\epsilon^2)$ are posed as

$$O(1): \quad \mathcal{L}_c \tilde{C}_0 = 0, \tag{C10}$$

$$O(\epsilon): \quad \mathcal{L}_c \tilde{C}_1 = u_x \frac{\partial \tilde{C}_0}{\partial \xi}, \tag{C11}$$

$$O(\epsilon^2): \quad \mathcal{L}_c \tilde{C}_2 = \frac{\partial \tilde{C}_0}{\partial \tau} + u_x \frac{\partial \tilde{C}_1}{\partial \xi} - \frac{\partial^2 \tilde{C}_0}{\partial \xi^2}. \tag{C12}$$

The boundary conditions of $\tilde{C}_i$ $(i = 0, 1, 2)$ are

$$\frac{\partial \tilde{C}_i}{\partial y} + \mathrm{Pe}_v \tilde{C}_i = \{\mathrm{Sh}\tilde{C}_i, 0\} \quad \text{at } y = \{0, 1\}. \tag{C13}$$

The solution to Eq. (C10) is written as

$$\tilde{C}_0(\xi, y, \tau) = f_0(y) c(\xi, \tau), \tag{C14}$$

where $f_0(y)$ is the eigenfunction in Appendix A associated with λ_0 and $c(\xi, \tau)$ is a function characterizing the longitudinal variation of concentration. One may understand $f_0(y)$ as the vertical concentration distribution (not normalized) and $c(\xi, \tau)$ as the temporal vertical average concentration at ξ (multiplied by a constant). It is evident that Eq. (C14) satisfies Eq. (C10).

The solution for $O(\epsilon)$ is

$$\tilde{C}_1(\xi, y, \tau) = \chi(y) \frac{\partial c}{\partial \xi} + f_0(y) g(\xi, \tau), \tag{C15}$$

where $g(\xi, \tau)$ is an undetermined function but is irrelevant to subsequent analysis; $\chi(y)$ is the first-order corrector; by substituting Eq. (C15) into Eq. (C11) one finds that $\chi(y)$ solves the cell problem

$$\mathcal{L}_c \chi = u_x(y) f_0(y), \tag{C16}$$

and $\overline{\chi} = 0$ is enforced to get a unique solution.

We denote

$$\langle A, B \rangle_w \triangleq \int_0^1 AB w(y) dy \tag{C17}$$

as the inner product with the weighting function $w(y)$ defined in Eq. (A5). The inner product of the left-hand side of Eq. (C11) and f_0 is

$$\begin{aligned} \langle \mathcal{L}_c \chi, f_0 \rangle_w &= \int_0^1 (\mathcal{L}\chi + \lambda_0 \chi) f_0 w \, dy \\ &= \int_0^1 [(\mathcal{L}_s \chi) f_0 + \lambda_0 w f_0 \chi] dy \\ &= \int_0^1 [(\mathcal{L}_s f_0) \chi + \lambda_0 w f_0 \chi] dy \\ &= 0, \end{aligned} \tag{C18}$$

where the self-adjointness of $\mathcal{L}_s$ is used to simplify the equation above. Thus the right-hand side of Eq. (C11) and f_0 must also equal zero, which yields the solvability condition,

$$\langle u_x f_0, f_0 \rangle_w = 0. \tag{C19}$$

The steady effective velocity is found to be

$$u_{\mathrm{eff}}^{\infty} = \frac{\langle u f_0, f_0 \rangle_w}{\overline{u}}. \tag{C20}$$

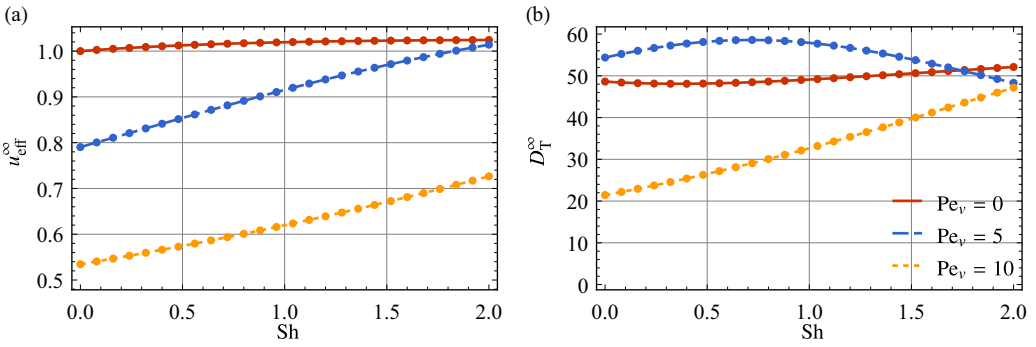

FIG. 13. Comparison of (a) steady effective velocity u_{eff}^{∞} and (b) steady dispersivity D_{T}^{∞} obtained with homogenization/GTD (dots) and method of moments (lines). $\text{Pe}_u = 100$ in all cases.

$\chi(y)$ is also subject to the boundary conditions (C13), and thus it can be also solved by eigenfunction expansion

$$\chi(y) = \sum_{i=0}^{N} k_i f_i(y), \tag{C21}$$

where

$$k_i = \frac{b}{\lambda_i - \lambda_0} \langle u_x f_0, f_i \rangle_w, \quad i = 1, 2, \ldots, N \tag{C22}$$

and k_0 is determined by the condition $\overline{\chi} = 0$.

Proceeding with the perturbation problem at $O(\epsilon^2)$, the solvability condition requires

$$\left\langle \frac{\partial \tilde{C}_0}{\partial \tau} + u_x \frac{\partial \tilde{C}_1}{\partial \xi} - \frac{\partial^2 \tilde{C}_0}{\partial \xi^2}, f_0 \right\rangle_w = 0, \tag{C23}$$

which simplifies to an effective diffusion equation for $c(\xi, \tau)$,

$$\frac{\partial c(\xi, \tau)}{\partial \tau} = (1 + D_{\text{e}}) \frac{\partial^2 c(\xi, \tau)}{\partial \xi^2}, \tag{C24}$$

equaling to

$$\frac{\partial c(x, t)}{\partial t} = (1 + D_{\text{e}}) \frac{\partial^2 c(x, t)}{\partial x^2}, \tag{C25}$$

where $D_{\text{e}} = -\langle u_x \chi, f_0 \rangle_w$ is the enhanced diffusivity. Converting back to the original nondimensionalized coordinates, the above equation becomes

$$\frac{\partial \overline{C}}{\partial t} + \text{Pe}_u \overline{u} u_{\text{eff}} \frac{\partial \overline{C}}{\partial x} = D_{\text{T}}^{\infty} \frac{\partial^2 \overline{C}}{\partial x^2} - \lambda_0 \overline{C}, \tag{C26}$$

where c is replaced by $\overline{C}$ and $1 + D_{\text{e}}$ is replaced by D_{T}^{∞}. This homogenized advection-diffusion equation approximately holds for $t \gg 1$. With a source initially located at $x = 0$, the solution for the equation above is its Green's function

$$\overline{C}(x, t) = \frac{1}{\sqrt{4 D_{\text{T}}^{\infty} t}} \exp\left[-\frac{(x - \text{Pe}_u \overline{u} u_{\text{eff}} t)^2}{4 D_{\text{T}}^{\infty} t} - \lambda_0 t \right]. \tag{C27}$$

The comparison of u_{eff}^{∞} and D_{T}^{∞} obtained with homogenization/GTD and method of moments is plotted in Fig. 13, showing good agreement.

[1] G. Taylor, Dispersion of soluble matter in solvent flowing slowly through a tube, Proc. R. Soc. A **219**, 186 (1953).
[2] H. B. Fischer, Longitudinal dispersion and turbulent mixing in open-channel flow, Annu. Rev. Fluid Mech. **5**, 59 (1973).
[3] H. B. Fischer, Mixing and dispersion in estuaries, Annu. Rev. Fluid Mech. **8**, 107 (1976).
[4] P. Wang and O. A. Cirpka, Surface transient storage under low-flow conditions in streams with rough bathymetry, Water Resour. Res. **57**, e2021WR029899 (2021).
[5] V. Hoshyargar, S. N. Ashrafizadeh, and A. Sadeghi, Mass transport characteristics of diffusioosmosis: Potential applications for liquid phase transportation and separation, Phys. Fluids **29**, 012001 (2017).
[6] R. E. Migacz and J. T. Ault, Diffusiophoresis in a Taylor-dispersing solute, Phys. Rev. Fluids **7**, 034202 (2022).
[7] W. Jiang and G. Chen, Dispersion of gyrotactic micro-organisms in pipe flows, J. Fluid Mech. **889**, A18 (2020).
[8] H. C. W. Chu, S. Garoff, R. D. Tilton, and A. S. Khair, Macrotransport theory for diffusiophoretic colloids and chemotactic microorganisms, J. Fluid Mech. **917**, A52 (2021).
[9] M. Guan, L. Zeng, C. F. Li, X. L. Guo, Y. H. Wu, and P. Wang, Transport model of active particles in a tidal wetland flow, J. Hydrol. **593**, 125812 (2021).
[10] B. Wang, W. Jiang, and G. Chen, Cross-channel distribution and streamwise dispersion of micro-swimmers in a vertical channel flow: A study on the effects of shear, particle shape, and convective inertial torque, Phys. Fluids **34**, 011904 (2022).
[11] B. Wang, W. Jiang, and G. Chen, Gyrotactic trapping of micro-swimmers in simple shear flows: A study directly from the fundamental Smoluchowski equation, J. Fluid Mech. **939**, A37 (2022).
[12] G. Taylor, The dispersion of matter in turbulent flow through a pipe, Proc. R. Soc. A **223**, 446 (1954).
[13] I. Frankel and H. Brenner, On the foundations of generalized Taylor dispersion theory, J. Fluid Mech. **204**, 97 (1989).
[14] H. Brenner and D. A. Edwards, *Macrotransport Processes*, Butterworth-Heinemann Series in Chemical Engineering (Butterworth-Heinemann, Stoneham, MA, 1993).
[15] R. Aris, On the dispersion of a solute in a fluid flowing through a tube, Proc. R. Soc. A **235**, 67 (1956).
[16] N. G. Barton, On the method of moments for solute dispersion, J. Fluid Mech. **126**, 205 (1983).
[17] W. N. Gill, A note on the solution of transient dispersion problems, Proc. R. Soc. A **298**, 335 (1967).
[18] R. Sankarasubramanian, W. N. Gill, and T. B. Benjamin, Unsteady convective diffusion with interphase mass transfer, Proc. R. Soc. A **333**, 115 (1973).
[19] P. Wang and G. Chen, Transverse concentration distribution in Taylor dispersion: Gill's method of series expansion supported by concentration moments, Int. J. Heat Mass Transfer **95**, 131 (2016).
[20] W. Q. Jiang and G. Q. Chen, Solution of Gill's generalized dispersion model: Solute transport in Poiseuille flow with wall absorption, Int. J. Heat Mass Transfer **127**, 34 (2018).
[21] J. Guo, W. Jiang, G. Chen, Z. Li, N. S. Alharbi, and M. Wakeel, Solute dispersion in an open channel turbulent flow: Solution by a generalized model, J. Hydrol. **604**, 127239 (2022).
[22] C. C. Mei, J.-L. Auriault, and C.-O. Ng, Some applications of the homogenization theory, Adv. Appl. Mech. **32**, 277 (1996).
[23] C.-O. Ng and T. L. Yip, Effects of kinetic sorptive exchange on solute transport in open-channel flow, J. Fluid Mech. **446**, 321 (2001).
[24] Z. Wu and G. Q. Chen, Approach to transverse uniformity of concentration distribution of a solute in a solvent flowing along a straight pipe, J. Fluid Mech. **740**, 196 (2014).
[25] A. H. Kumar, S. J. Thomson, T. R. Powers, and D. M. Harris, Taylor dispersion of elongated rods, Phys. Rev. Fluids **6**, 094501 (2021).
[26] P. C. Chatwin, The approach to normality of the concentration distribution of a solute in a solvent flowing along a straight pipe, J. Fluid Mech. **43**, 321 (1970).
[27] B. Ling, A. M. Tartakovsky, and I. Battiato, Dispersion controlled by permeable surfaces: Surface properties and scaling, J. Fluid Mech. **801**, 13 (2016).
[28] B. Ling, C. B. Rizzo, I. Battiato, and F. P. J. de Barros, Macroscale transport in channel-matrix systems via integral transforms, Phys. Rev. Fluids **6**, 044501 (2021).

[29] J. Guo, W. Jiang, L. Zhang, Z. Li, and G. Chen, Effect of bed absorption on contaminant transport in wetland channel with rectangular cross-section, J. Hydrol. **578**, 124078 (2019).
[30] Z. Wu, E. Foufoula-Georgiou, G. Parker, A. Singh, X. Fu, and G. Wang, Analytical solution for anomalous diffusion of bedload tracers gradually undergoing burial, J. Geophys. Res. Earth Surf. **124**, 21 (2019).
[31] Z. Wu, A. Singh, X. Fu, and G. Wang, Transient anomalous diffusion and advective slowdown of bedload tracers by particle burial and exhumation, Water Resour. Res. **55**, 7964 (2019).
[32] R. H. Davis and J. D. Sherwood, A similarity solution for steady-state crossflow microfiltration, Chem. Eng. Sci. **45**, 3203 (1990).
[33] K. Jayaraj and R. S. Subramanian, On relaxation phenomena in field-flow fractionation, Sep. Sci. Technol. **13**, 791 (1978).
[34] R. Smith, Vertical drift and reaction effects upon contaminant dispersion in parallel shear flows, J. Fluid Mech. **165**, 425 (1986).
[35] T. Y. Lin and E. S. G. Shaqfeh, Taylor dispersion in the presence of cross flow and interfacial mass transfer, Phys. Rev. Fluids **4**, 034501 (2019).
[36] M. Shapiro and H. Brenner, Chemically reactive generalized Taylor dispersion phenomena, AIChE J. **33**, 1155 (1987).
[37] G. K. Batchelor, *An Introduction to Fluid Dynamics* (Cambridge University Press, New York, 2000).
[38] W. Jiang and G. Chen, Transient dispersion process of active particles, J. Fluid Mech. **927**, A11 (2021).
[39] S. Blinnikov and R. Moessner, Expansions for nearly Gaussian distributions, Astron. Astrophys. Suppl. Ser. **130**, 193 (1998).
[40] R. Smith, Gaussian approximation for contaminant dispersion, Q. J. Mech. Appl. Math. **35**, 345 (1982).
[41] R. Smith, The contraction of contaminant distributions in reversing flows, J. Fluid Mech. **129**, 137 (1983).
[42] M. Shapiro and H. Brenner, Taylor dispersion of chemically reactive species: Irreversible first-order reactions in bulk and on boundaries, Chem. Eng. Sci. **41**, 1417 (1986).
[43] R. Erban and S. J. Chapman, Reactive boundary conditions for stochastic simulations of reaction–diffusion processes, Phys. Biol. **4**, 16 (2007).
[44] A. Singer, Z. Schuss, A. Osipov, and D. Holcman, Partially reflected diffusion, SIAM J. Appl. Math. **68**, 844 (2008).
[45] R. Mauri, Dispersion, convection, and reaction in porous media, Phys. Fluids **3**, 743 (1991).
[46] G. A. Pavliotis and A. M. Stuart, *Multiscale Methods: Averaging and Homogenization*, Texts Applied in Mathematics, Vol. 53 (Springer, New York, 2008).
[47] H. Chen and J.-L. Thiffeault, Shape matters: A Brownian microswimmer in a channel, J. Fluid Mech. **916**, A15 (2021).
[48] J. Rubinstein and R. Mauri, Dispersion and convection in periodic porous media, SIAM J. Appl. Math. **46**, 1018 (1986).